LETTER

doi:10.1038/nature14491

Ocean impact on decadal Atlantic climate variability revealed by sea-level observations

Gerard D. McCarthy[1], Ivan D. Haigh[2], Joël J.-M. Hirschi[1], Jeremy P. Grist[1] & David A. Smeed[1]

Decadal variability is a notable feature of the Atlantic Ocean and the climate of the regions it influences. Prominently, this is manifested in the Atlantic Multidecadal Oscillation (AMO) in sea surface temperatures. Positive (negative) phases of the AMO coincide with warmer (colder) North Atlantic sea surface temperatures. The AMO is linked with decadal climate fluctuations, such as Indian and Sahel rainfall[1], European summer precipitation[2], Atlantic hurricanes[3] and variations in global temperatures[4]. It is widely believed that ocean circulation drives the phase changes of the AMO by controlling ocean heat content[5]. However, there are no direct observations of ocean circulation of sufficient length to support this, leading to questions about whether the AMO is controlled from another source[6]. Here we provide observational evidence of the widely hypothesized link between ocean circulation and the AMO. We take a new approach, using sea level along the east coast of the United States to estimate ocean circulation on decadal timescales. We show that ocean circulation responds to the first mode of Atlantic atmospheric forcing, the North Atlantic Oscillation, through circulation changes between the subtropical and subpolar gyres—the intergyre region[7]. These circulation changes affect the decadal evolution of North Atlantic heat content and, consequently, the phases of the AMO. The Atlantic overturning circulation is declining[8] and the AMO is moving to a negative phase. This may offer a brief respite from the persistent rise of global temperatures[4], but in the coupled system we describe, there are compensating effects. In this case, the negative AMO is associated with a continued acceleration of sea-level rise along the northeast coast of the United States[9,10].

The difficulty in linking ocean circulation changes to decadal climate variations lies in the fact that long observational records of ocean transports are rare. Measurements such as those of the Florida Current since 1982[11] and the Greenland–Scotland ridge transports[12] since the mid-1990s are some of the longest continuous ocean transport records available. Continuous, full-depth, basin-wide measurements of the Atlantic overturning circulation only began in 2004 with the RAPID monitoring project at 26° N (ref. 13). None of these records are long enough to directly link ocean circulation with decadal climate variations such as the AMO.

Sea-level measurements from tide gauges provide an integrated measure of water column properties and offer timeseries of sufficient length (Extended Data Fig. 1) to study decadal ocean circulation variations. Investigating ocean circulation using tide gauges is not new: the first attempt to estimate the Gulf Stream using tide gauges was made in 1938[14]. The principle is based on geostrophic dynamics: on timescales longer than a few days, ocean circulation is in geostrophic balance so, looking downstream, the sea level is seen to increase from left to right in the Northern Hemisphere.

Estimates of the Gulf Stream using tide gauges have focused on the American east coast, with an offshore estimate of sea level from either an island gauge[15] or a reconstructed sea level[16]. A weakness of this method is that the offshore measurement lies in the eddy-filled ocean where sea-level fluctuations at any one point are influenced by mesoscale variations[17] even on long timescales, increasing the difficulty of making estimates of ocean circulation that are coherent on large spatial scales. This is the case for sea level at Bermuda, whose decadal fluctuations can be reproduced by considering a Rossby wave response to wind forcing[16]. To make estimates of ocean circulation that capture the fluctuations in large-scale circulation and are less affected by eddy variability, measurements close to or on the western boundary are necessary[18]. We account for this by focusing on the gradient of sea level along the US east coast. Here the mean dynamic sea level decreases to the north (Fig. 1a) due to the transition from subtropical to subpolar gyres. This dynamic gradient reflects a circulation that contains elements not only of the Gulf Stream but also of cold, subpolar water from the north, primarily associated with the overturning circulation[19]. Indeed, in model simulations, this meridional gradient of sea level along this coast responds strongly to declines in the Atlantic overturning circulation[20]. Ultimately, it is the heat transport that we are interested in. And while the overturning circulation carries about 90% of the heat at subtropical latitudes[21], ocean heat transport at the latitude of the intergyre region consists of similar contributions from both the overturning circulation and the gyre circulation[22]. For this reason, we do not discuss separately overturning and gyre but only ocean circulation in this intergyre region, which contains elements of both mechanisms.

Sea-level fluctuations from Florida to Boston divide into two coherent groups either side of Cape Hatteras[23] (Extended Data Figs 2, 3). This large-scale coherence in sea level is driven by ocean circulation. North of Cape Hatteras, coherent sea-level fluctuations have been linked with fluctuations in the overturning circulation[19,24]. South of Cape Hatteras, fluctuations in the Gulf Stream from Florida to Cape Hatteras are reflected in sea-level fluctuations. As Cape Hatteras marks the boundary between the subtropical and subpolar gyres on this coastline (Fig. 1a), we can construct a single sea-level composite representative of the subtropical (subpolar) circulation by averaging sea level from linearly detrended, deseasonalized tide gauges, with the inverse barometer effect removed, south (north) of the Cape (Fig. 1b, c). The difference, south minus north (Fig. 1d), represents our circulation index. This index projects onto observed surface velocities during the satellite era in the intergyre region, with a positive index associated with more northwards flow and a more northerly path of this circulation (Extended Data Fig. 4). Similarly, in a high-resolution ocean model, over timescales that contain both the cool phase of the AMO in the 1970s[25] and the warm phase of the 1990s[26], the sea-level index projects onto a similar pattern of circulation, with a positive index associated with more northward heat transport (Extended Data Fig. 5).

Ocean circulation is proportional to heat transport at both subtropical and subpolar latitudes[22]. A number of recent studies (see, for example, ref. 27) have emphasized the dominant role of ocean heat transport in heat content changes, relating the accumulation (in time) of heat transport to heat content. This suggests that the accumulation of our sea-level index across Cape Hatteras, as a proxy for ocean circulation, can be related to ocean heat content. The largest AMO

[1]National Oceanography Centre, University of Southampton Waterfront Campus, European Way, Southampton SO14 3ZH, UK. [2]Ocean and Earth Science, National Oceanography Centre, University of Southampton Waterfront Campus, European Way, Southampton SO14 3ZH, UK.

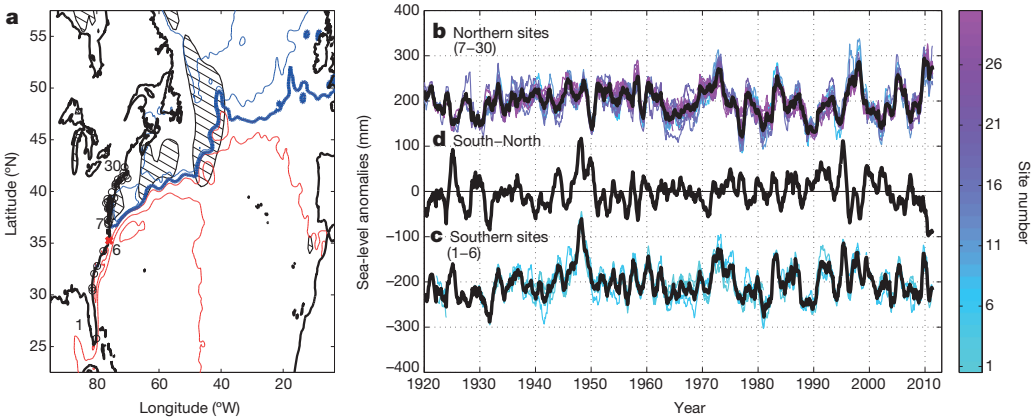

Figure 1 | Dynamic sea level and circulation along the western Atlantic seaboard. **a**, Negative (positive) mean dynamic topography contours in blue (red) indicate cyclonic (anticyclonic) geostrophic streamlines. Contour values in metres shown in Fig. 2. The zero contour (dark blue) marks the boundary between the subtropical and subpolar gyres. Hatched areas indicate warm sea surface temperature anomalies of greater than 0.5 °C during the positive phase of the AMO from 1995–2004 relative to from 1961–2012. **b**, **c**, Dynamic sea-level anomalies north (**b**; sites 7–30, +200 mm offset) and south (**c**; sites 1–6, −200 mm offset) of Cape Hatteras, with averages in black. **d**, The difference in sea level, southern minus northern average, defines our sea-level index for ocean circulation.

signal is in the subpolar region (Fig. 1a), so we wish to show that, as a measure of ocean circulation, our sea-level index is related to heat transport into the subpolar gyre and consequently heat content changes there. Such a mechanism is supported by our model, in which the sea-level index leads the heat transport into the subpolar gyre at 40° N and, consequently, leads the heat content changes there (Extended Data Fig. 6).

Although we do not have observations of heat transport, we can relate our sea-level index directly to the heat content changes in the subpolar gyre since 1960. Figure 2a shows the accumulated sea-level index (blue curve), together with a direct estimate of the heat content in the area in the depth-weighted temperature anomaly in the top 500 m between 40° N and 60° N (black line). Heat content trends are similar throughout the upper 1,000 m of the Atlantic, below which they reverse due to the depth structure of the Atlantic overturning circulation. The cool subpolar upper ocean of the 1970s and 1980s and subsequent warming in the 1990s is captured by the accumulated sea-level index, observationally supporting the hypothesis that circulation changes and not only air–sea fluxes were involved in these changes[28]. For the purposes of statistical analyses, the timeseries have had a 7-year low-pass, Tukey filter applied to them, which is referred to by the prefix '7-year' from here on. The 7-year sea-level index leads the 7-year rate of heat content change by 2 years with a maximum correlation of 0.58 (significant at the 95% level). The reason that the accumulated sea-level index leads the large rise in heat content from 40° N to 60° N in the early 1990s can be interpreted by looking at maps of the heat content anomaly evolution. Heat content builds downstream of the intergyre region from the mid-1980s to the mid-1990s (Fig. 2b). This heat content anomaly is then observed downstream in the subpolar gyre in the late 1990s and early 2000s (Fig. 2c), indicating that the sea-level index could provide an early indication of subpolar heat content change.

The first mode of atmospheric variability over the North Atlantic, the North Atlantic Oscillation (NAO), forces both buoyancy and wind-driven ocean circulation[7] and, we believe, is the major forcing of the circulation in the intergyre region. The 7-year NAO is significantly correlated with (r = 0.71 at the 98% level) and leads the 7-year sea-level difference by approximately 1 year over the period 1950 to 2012. On extending the time period to 1920–2012, the correlation drops slightly but is still significantly correlated (r = 0.61 at the 98% level, Extended Data Fig. 7). The correlation between the sea-level difference and the NAO is higher and more significant than the correlation of the NAO with either the southern or northern sea-level (Fig. 1b, c) composites (r = −0.5 at the 86% level for the southern composite; r = −0.43 at the 70% level for the northern); this supports

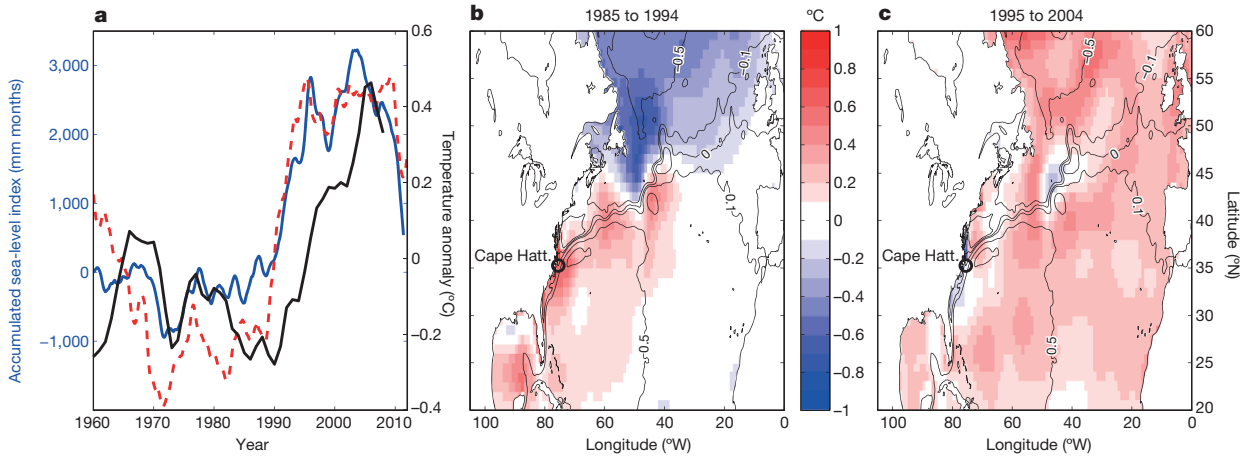

Figure 2 | Relating the sea-level circulation index to heat content changes. **a**, Accumulated sea-level index (nominally, in mm month) derived from accumulating the sea-level circulation index (blue), temperature anomaly in the upper 500 m of the subpolar North Atlantic from 40° to 60° N (black) and accumulated NAO (red, dashed). **b**, Average temperature anomaly in the top 500 m for the periods 1985–94 relative to the average from 1958–2010. Contours of mean dynamic topography (metres) defined in Fig. 1a are overlaid for reference. **c**, Same as **b** but for the period 1995–2004.

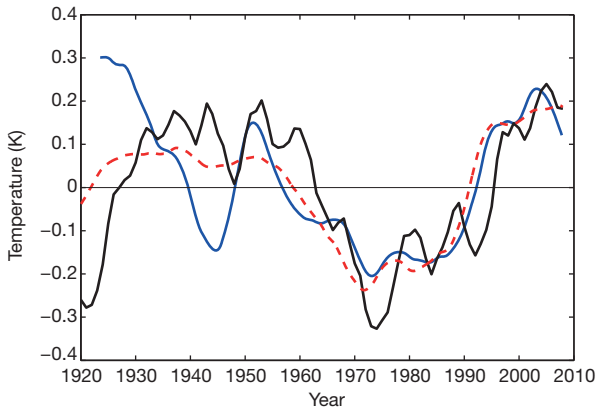

Figure 3 | Sea-level circulation index, the NAO and the AMO on multi-decadal timescales. Shown are the accumulated sea-level index (blue), which is representative of subpolar heat content evolution, the accumulated NAO (red, dashed) and the AMO (black). The heat content proxy and the accumulated NAO have been normalized. All timeseries have been 7-year low-pass filtered. The accumulated sea-level index and accumulated NAO have been detrended.

our hypothesis that the NAO forces the ocean circulation and consequently the ocean heat transport into the subpolar gyre.

In the past 90 years, the AMO has undergone three major transitions: warming in the mid-1990s and 1920s, and a cooling in the 1960s. From the early-1920s, when the tide gauge network along the east coast of North America was developed, robust comparisons of our sea-level index to the AMO are possible (Fig. 3). The accumulated sea-level index and the accumulated NAO are linearly detrended and capture much of the multi-decadal variation. The 7-year sea-level index leads the 7-year rate of change of the AMO by 2 years and is significantly correlated ($r = 0.51$, significant at the 96% level, Extended Data Fig. 8). This lead time of 2 years remains consistent when the timeseries is broken into 60-year blocks (Extended Data Table 2). In recent years, the sea-level index (Fig. 1d) indicates that the AMO is again transitioning to a negative phase, consistent with observations of a reduced overturning circulation[8].

Using the sea-level difference between subtropical and subpolar gyres, we have developed and validated a proxy for ocean circulation in the intergyre region. This represents a mechanism for ocean heat transport to the subpolar gyre and heat content changes there. When observations exist, heat content changes have coincided with the major phase transitions of the AMO, confirming that ocean circulation plays a key role in decadal Atlantic variability. The ocean responds to NAO forcing with changes in ocean circulation: on decadal timescales, the ocean integrates NAO forcing and returns it to the atmosphere as the AMO. This is implicitly the Bjerknes compensation that had previously been seen in air–sea fluxes[29]. The sea-level difference provides an indicator of ocean circulation changes that precede phase changes in the AMO, thus explaining why, as the positive AMO declines[4], sea-level rise is accelerating north of Cape Hatteras[9,10]. While Greenland ice sheet melt has been linked with accelerating sea-level rise in recent years, the fact that the period of accelerated sea-level rise from the 1950s to the 1970s[10] (as well as the current period of sea-level rise) coincides with a declining AMO indicates that multi-decadal fluctuations in ocean circulation play a key role. In this framework, sea-level rise along the US east coast becomes entwined with the effects of the AMO on climate.

Online Content Methods, along with any additional Extended Data display items and Source Data, are available in the online version of the paper; references unique to these sections appear only in the online paper.

Received 3 July 2014; accepted 8 April 2015.

1. Zhang, R. & Delworth, T. L. Impact of Atlantic multidecadal oscillations on India/Sahel rainfall and Atlantic hurricanes. *Geophys. Res. Lett.* **34,** L23708 (2006).
2. Sutton, R. T. & Dong, B. Atlantic Ocean influence on a shift in European climate in the 1990s. *Nature Geosci.* **5,** 788–792 (2012).
3. Goldenberg, S. B., Landsea, C. W., Mestas-Nuñez, A. M. & Gray, W. M. The recent increase in Atlantic hurricane activity: causes and implications. *Science* **293,** 474–479 (2001).
4. Chen, X. & Tung, K.-K. Varying planetary heat sink led to global-warming slowdown and acceleration. *Science* **345,** 897–903 (2014).
5. Delworth, T. L. & Mann, M. E. Observed and simulated multidecadal variability in the Northern Hemisphere. *Clim. Dyn.* **16,** 661–676 (2000).
6. Booth, B. B., Dunstone, N. J., Halloran, P. R., Andrews, T. & Bellouin, N. Aerosols implicated as a prime driver of twentieth-century North Atlantic climate variability. *Nature* **484,** 228–232 (2012).
7. Marshall, J., Johnson, H. & Goodman, J. A study of the interaction of the North Atlantic Oscillation with ocean circulation. *J. Clim.* **14,** 1399–1421 (2001).
8. Smeed, D. A. *et al.* Observed decline of the Atlantic Meridional Overturning Circulation 2004 to 2012. *Ocean Science* **10,** 39–38 (2014).
9. Sallenger, A. H. Jr, Doran, K. S. & Howd, P. A. Hotspot of accelerated sea-level rise on the Atlantic coast of North America. *Nature Clim. Change* **2,** 884–888 (2012).
10. Boon, J. D. Evidence of sea level acceleration at US and Canadian tide stations, Atlantic Coast, North America. *J. Coast. Res.* **28,** 1437–1445 (2012).
11. Meinen, C. S., Baringer, M. O. & Garcia, R. F. Florida Current transport variability: an analysis of annual and longer-period signals. *Deep Sea Res. I* **57,** 835–846 (2010).
12. Østerhus, S., Turrell, W. R., Jónsson, S. & Hansen, B. Measured volume, heat, and salt fluxes from the Atlantic to the Arctic Mediterranean. *Geophys. Res. Lett.* **32,** L07603 (2005).
13. McCarthy, G. D. *et al.* Measuring the Atlantic Meridional Overturning Circulation at 26°N. *Prog. Oceanogr.* **130,** 91–111 (2015).
14. Montgomery, R. Fluctuations in monthly sea level on eastern US coast as related to dynamics of western North Atlantic Ocean. *J. Mar. Res.* **1,** 165–185 (1938).
15. Iselin, C. O. Preliminary report on long-period variations in the transport of the Gulf Stream system. *Pap. Phys. Oceanogr. Meteorol.* **3,** 1–40 (1940).
16. Sturges, W. & Hong, B. Wind forcing of the Atlantic thermocline along 32°N at low frequencies. *J. Phys. Oceanogr.* **25,** 1706–1715 (1995).
17. Wunsch, C. Mass and volume transport variability in an eddy-filled ocean. *Nature Geosci.* **1,** 165–168 (2008).
18. Kanzow, T. *et al.* Basinwide integrated volume transports in an eddy-filled ocean. *J. Phys. Oceanogr.* **39,** 3091–3110 (2009).
19. Bingham, R. J. & Hughes, C. W. Signature of the Atlantic meridional overturning circulation in sea level along the east coast of North America. *Geophys. Res. Lett.* **36,** L02603 (2009).
20. Yin, J., Schlesinger, M. E. & Stouffer, R. J. Model projections of rapid sea-level rise on the northeast coast of the United States. *Nature Geosci.* **2,** 262–266 (2009).
21. Johns, W. E. *et al.* Continuous, array-based estimates of Atlantic Ocean heat transport at 26.5°N. *J. Clim.* **24,** 2429–2449 (2011).
22. Grist, J. P. *et al.* The roles of surface heat flux and ocean heat transport convergence in determining Atlantic Ocean temperature variability. *Ocean Dyn.* **60,** 771–790 (2010).
23. Thompson, P. & Mitchum, G. Coherent sea level variability on the North Atlantic western boundary. *J. Geophys. Res.* **119,** 5676–5689 (2014).
24. Ezer, T. Sea level rise, spatially uneven and temporally unsteady: why the US east coast, the global tide gauge record and the global altimeter data show different trends. *Geophys. Res. Lett.* **40,** 5439–5444 (2013).
25. Hodson, D. L., Robson, J. I. & Sutton, R. T. An anatomy of the cooling of the North Atlantic Ocean in the 1960s and 1970s. *J. Clim.* **27,** 8229–8243 (2014).
26. Häkkinen, S. & Rhines, P. B. Decline of subpolar North Atlantic circulation during the 1990s. *Science* **304,** 555–559 (2004).
27. Bryden, H. L., King, B. A., McCarthy, G. D. & McDonagh, E. L. Impact of a 30% reduction in Atlantic meridional overturning during 2009–2010. *Ocean Sci.* **10,** 683–691 (2014).
28. Robson, J., Sutton, R., Lohmann, K., Smith, D. & Palmer, M. D. Causes of the rapid warming of the North Atlantic Ocean in the mid-1990s. *J. Clim.* **25,** 4116–4134 (2012).
29. Gulev, S., Latif, M., Keenlyside, N. S. & Koltermann, K. North Atlantic Ocean control on surface heat flux at multidecadal timescale. *Nature* **499,** 464–467 (2013).

Acknowledgements G.D.M. and D.A.S. are supported by the UK Natural Environment Research Council (NERC) RAPID-WATCH programme. I.D.H. was partly supported by the UK NERC consortium project iGlass (NE/I009906/1). J.P.G. and J.J.-M.H. are supported by NERC National Capability funding.

Author Contributions G.D.M. originated and developed the concept. I.D.H. provided the tide gauge data analysis. J.P.G. and J.J.-M.H. provided the numerical model analysis. D.A.S. carried out the statistical analysis. All authors contributed to the shaping and production of the manuscript

Author Information Comma-separated data used in the manuscript are available to download from http://bit.ly/1F7gtps. Reprints and permissions information is available at www.nature.com/reprints. The authors declare no competing financial interests. Readers are welcome to comment on the online version of the paper. Correspondence and requests for materials should be addressed to G.D.M. (gerard.mccarthy@noc.ac.uk).

METHODS

Data. Monthly mean sea-level records were obtained from the Permanent Service for Mean Sea-level (www.psmsl.org) for tide gauges stretching from Florida to Boston (locations 1 to 30, Extended Data Fig. 1). Linear trends were removed from each record. This removes the impact of glacial isostatic adjustment and other land subsidence effects, which have time periods of thousands of years and are known to affect tide gauges along this coastline. A 12-month low-pass filter removed the seasonal cycle. Southern (northern) composites of sea level were calculated by averaging records 1–6 (7–30). The meridional coherence of sea-level fluctuations is such that using just a single tide gauge results in an r.m.s. error of only 5 mm relative to the full composite. Finally, the sea-level index is simply the difference obtained by subtracting the northern from the southern sea-level composite. The high level of meridional coherence allows the interpretation of the sea-level gradient as this simple index.

Sources. Monthly NAO data from the National Center for Atmospheric Research "The Climate Data Guide: Hurrell North Atlantic Oscillation (NAO) Index (PC-based)" (https://climatedataguide.ucar.edu/climate-data/hurrell-north-atlantic-oscillation-nao-index-pc-based); monthly AMO index, based on the Kaplan sea surface temperature (SST) data set (from http://www.esrl.noaa.gov/psd/data/timeseries/AMO/); subsurface temperature data from the EN3 product (http://www.metoffice.gov.uk/hadobs/en3/); geostrophic velocity anomalies were produced and distributed by Aviso (http://www.aviso.altimetry.fr/) as part of the Ssalto ground processing segment. CNES-CLS09 Mean Dynamic Topography (v1.1 release) for the period 1993–99 was produced by the French Space Agency CNES.

Model validation. The multi-decadal oscillation of SSTs is most intense in the subpolar gyre (Fig. 1a). Modelling studies have shown that it is ocean heat transport into the subpolar gyre (here we choose 40° N) that controls the heat content of the subpolar upper ocean and consequently the SST. The concept here is that circulation in the intergyre region reflects the balance between warm subtropical water entering the subpolar gyre and colder subpolar water being recirculated within the gyre. We show that the sea-level gradient along the US east coast is a good proxy for this circulation (Extended Data Figs 4 and 5).

We can relate sea-level changes to ocean circulation in a reduced gravity geostrophic framework:

$$\boldsymbol{v} = \frac{\boldsymbol{g}'}{\boldsymbol{f}}\boldsymbol{k} \times \nabla \boldsymbol{h}$$

where $\boldsymbol{v}$ is geostrophic velocity, $\boldsymbol{k}$ is the unit vector in the vertical direction, $\boldsymbol{h}$ is sea level, $\boldsymbol{g}'$ is reduced gravity and $\boldsymbol{f}$ is the Coriolis parameter. To estimate the transport in the intergyre region, previous studies have considered the sea-level difference between an onshore tide gauge and an offshore tide gauge, such as Bermuda. Reference 24, for example, relates the sea-level difference between Atlantic City and Bermuda to the Atlantic overturning circulation.

However, Bermuda is in the eddy-filled ocean interior[17], which can disrupt spatially-coherent ocean transport signals. Our approach is to use sea-level estimates south of Cape Hatteras instead of an offshore sea-level estimate. Dynamic topography along the US east coast also decreases to the north across the intergyre boundary at Cape Hatteras much as it decreases from Bermuda to Atlantic City. However, measurements on the coast do not suffer the same contamination due to eddies as mid-ocean measurements[18]. Hence we estimate the transport along the intergyre boundary as:

$$v_{\mathrm{ig}} \propto h_{\mathrm{s}} - h_{\mathrm{n}}$$

where the subscript ig refers to the intergyre region, s and n refer to south and north respectively. We can formulate the heat transport through a section straddling the intergyre boundary as:

$$\mathrm{HT}_{\mathrm{ig}} = \rho c_p \iint \Theta v_{\mathrm{ig}} \mathrm{d}A$$

where ρ is density, c_p is the specific heat capacity of seawater, Θ is conservative temperature and A is the area of the section considered. In this study we assume that the velocity fluctuations dominate the temperature fluctuations and so set the heat transport directly proportional to the intergyre velocity. This is an assumption that has proved true in direct heat transport estimates[21]. We note there is no dilemma in picking the location of the northern or southern points as the meridional coherence of sea-level fluctuations allows us to use a simple average of all sea-level records from Miami Beach to Cape Hatteras (Cape Hatteras to Boston) for h_{s} (h_{n}).

In terms of upper ocean heat content, the heat transported in this intergyre region has a profound impact on the subpolar gyre. This is because warm water may be transferred from the upper waters of the subtropics to the subpolar gyre whereas subpolar water can only enter the subtropics at depth (traditionally in the deep western boundary current). Therefore we relate the heat transport into the subpolar gyre and heat content of the upper waters of the subpolar gyre to the transport in the intergyre region:

$$\mathrm{HT}_{40^{\circ}\mathrm{N}} \propto h_{\mathrm{s}} - h_{\mathrm{n}}$$

For exactly the reason that we need to use tide gauges as a proxy for heat transport, we cannot validate the conceptual model directly due to the lack of direct observations. However, a global eddy-permitting (1/4°) ocean model (ORCA-025) provides the framework to investigate these balances. The heat transport into the subpolar gyre has previously been shown in this model to be the dominant factor in setting upper ocean temperature in the subpolar gyre[22]. Here, we reproduce this result, showing that the accumulated heat transport across 40° N captures the major decadal fluctuations in heat content of the subpolar gyre (Extended Data Fig. 6). We can use these heat transport measurements to validate our circulation index. At this resolution there are shortcomings in the representation of the Gulf Stream path: the Gulf Stream overshoots at Cape Hatteras and separates from the US coast too far north. However, we take account of this in choosing the northern and southern sea-level points so that they straddle the separation point. Also, despite the model being eddy-permitting rather than eddy-resolving, it does generate mesoscale variability. This is seen when including an offshore sea-level measurement (such as Bermuda) in a sea-level circulation index. Such an index fails to reflect the large scale circulation. This effect would be expected to be even larger in an eddy-resolving model. Extended Data Fig. 5 shows that the model-derived sea-level index projects onto the intergyre velocities in a similar manner to the observed sea-level index. Extended Data Fig. 6 shows the accumulated sea-level difference compared with the accumulated heat transport across a section near 40° N and the volume averaged temperature of the upper 500 m of the subpolar gyre (40° N to 60° N). The sea-level difference is significantly correlated with the heat transport into the subpolar gyre ($r = 0.62$) and leads by 5 years (as in the main text, we report statistics on unaccumulated timeseries).

Code availability. Matlab code is available to download from http://bit.ly/1F7gtps.

Statistical analysis. Cross-correlations are calculated using annually averaged data after first removing the mean and linear trend from each variable. Two approaches are used to quantify the uncertainty in the correlation. First, we calculated the parameter

$$T = \sqrt{(N-2)}\,\frac{r}{\sqrt{1-r^2}}$$

where r is the correlation and N is the number of samples. The distribution of T is assumed to have a t-distribution with $N-2$ degrees of freedom when the samples are not autocorrelated. This is used with a one-sided test to estimate the likelihood that the correlation has not occurred by chance (that is, the certainty with which we can reject the null hypothesis). Our data are autocorrelated and the number of independent samples (degrees of freedom) is therefore smaller than N. To calculate the effective number of degrees of freedom we follow ref. 30 by evaluating the autocorrelation of each variable and the estimate N as

$$N_{\mathrm{eff}} = N_{\mathrm{obs}}\,\frac{(1-a_1 a_2)}{(1+a_1 a_2)}$$

where N_{eff} is the degrees of freedom, N_{obs} is the number of observations and a_1, a_2 are the values of the autocorrelations at a lag of one year. We evaluated N_{eff} over the longest time for each variable and then used the lowest value for all correlations. For the shorter time series N_{eff} was reduced in proportion to the length of the series. Degrees of freedom are reported in Extended Data Table 1.

In a second approach we applied the non-parametric method described in ref. 31. A large number (we used 10,000) of simulated time series are constructed from the Fourier transform of one of the original data series by preserving the modulus of each Fourier component but changing the phase to a random value between 0 and 2π. The distribution of correlations between these random series and the second variable was then calculated. The percentage of simulated correlations that are less than the observed correlation indicates the confidence that the true correlation is greater than zero. Because we are considering lagged correlations we modify the technique of ref. 31 so that for each simulated time series we evaluate the maximum of cross-correlation across all lags rather than the correlation at zero lag only. This provides a more stringent test of confidence.

To estimate the uncertainty in the time lag of the maximum correlation we used the times at which the correlation was equal to the maximum value less the

standard deviation of correlations derived from the simulated time series. The results are summarized in Extended Data Table 1.

We have also evaluated the correlation over shorter periods to determine if the lag has remained constant over time. Results from three overlapping 60-year periods are shown in Extended Data Table 2. For each the correlation is a maximum when sea-level difference leads the differentiated AMO by 2 to 3 years.

The text refers to both accumulated and unaccumulated timeseries. Accumulation of zero mean timeseries constrains the beginning and end of the accumulated timeseries to zero. To avoid this arbitrary constraint, we report all our statistics on unaccumulated timeseries. As mentioned, for the purposes of statistical analyses, the timeseries have had a 7-year, Tukey filter applied to them, which is referred to in the text with the prefix '7-year'.

Sample size. The timespan of the study was the maximum for which all of the necessary data were available. Therefore no statistical methods were used to predetermine sample size as we used all the samples available to us.

30. Bretherton, C. S., Widmann, M., Dymnikov, V. P., Wallace, J. M. & Bladé, I. The effective number of spatial degrees of freedom of a time-varying field. *J. Clim.* **12,** 1990–2009 (1999).
31. Ebisuzaki, W. A method to estimate the statistical significance of a correlation when the data are serially correlated. *J. Clim.* **10,** 2147–2153 (1997).

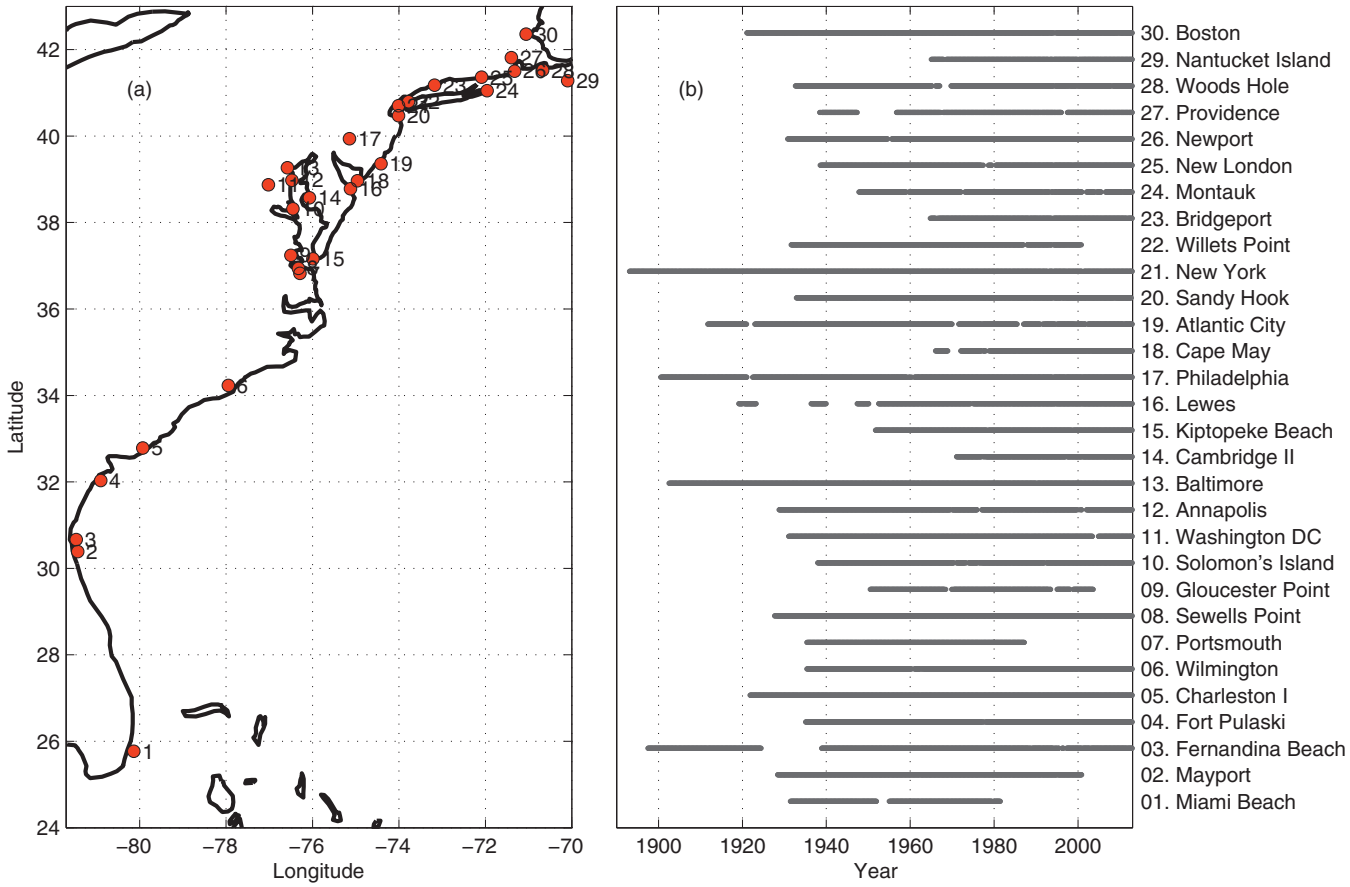

Extended Data Figure 1 | Tide gauges used in this study. **a**, Locations and **b**, temporal coverage of the tide gauges used in this study.

Extended Data Figure 2 | Dynamic sea-level anomalies from the 30 stations used in this study. Linear trends were removed from each record. This removes the impact of glacial isostatic adjustment and other land subsidence effects, which have time periods of thousands of years and are known to affect tide gauges along this coastline. A seasonal cycle was removed using a 12-month boxcar filter. From 1920, there are multiple tide gauges both north and south of Cape Hatteras, so this is when we begin our study.

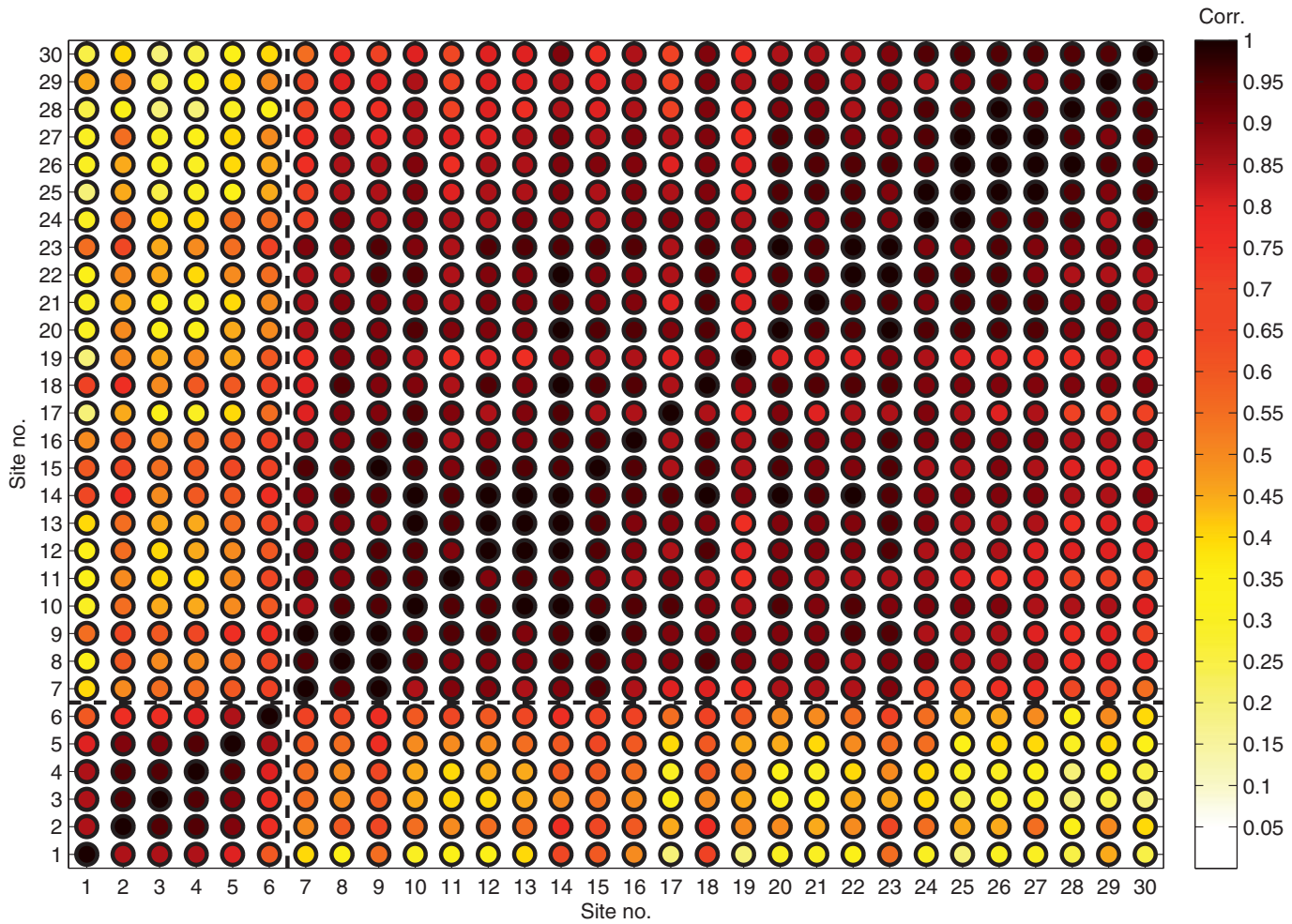

Extended Data Figure 3 | Correlation of tide gauges along the US east coast relative to one another. The dashed line indicates the location of Cape Hatteras. There is high correlation between tide gauges grouped north and south of Cape Hatteras.

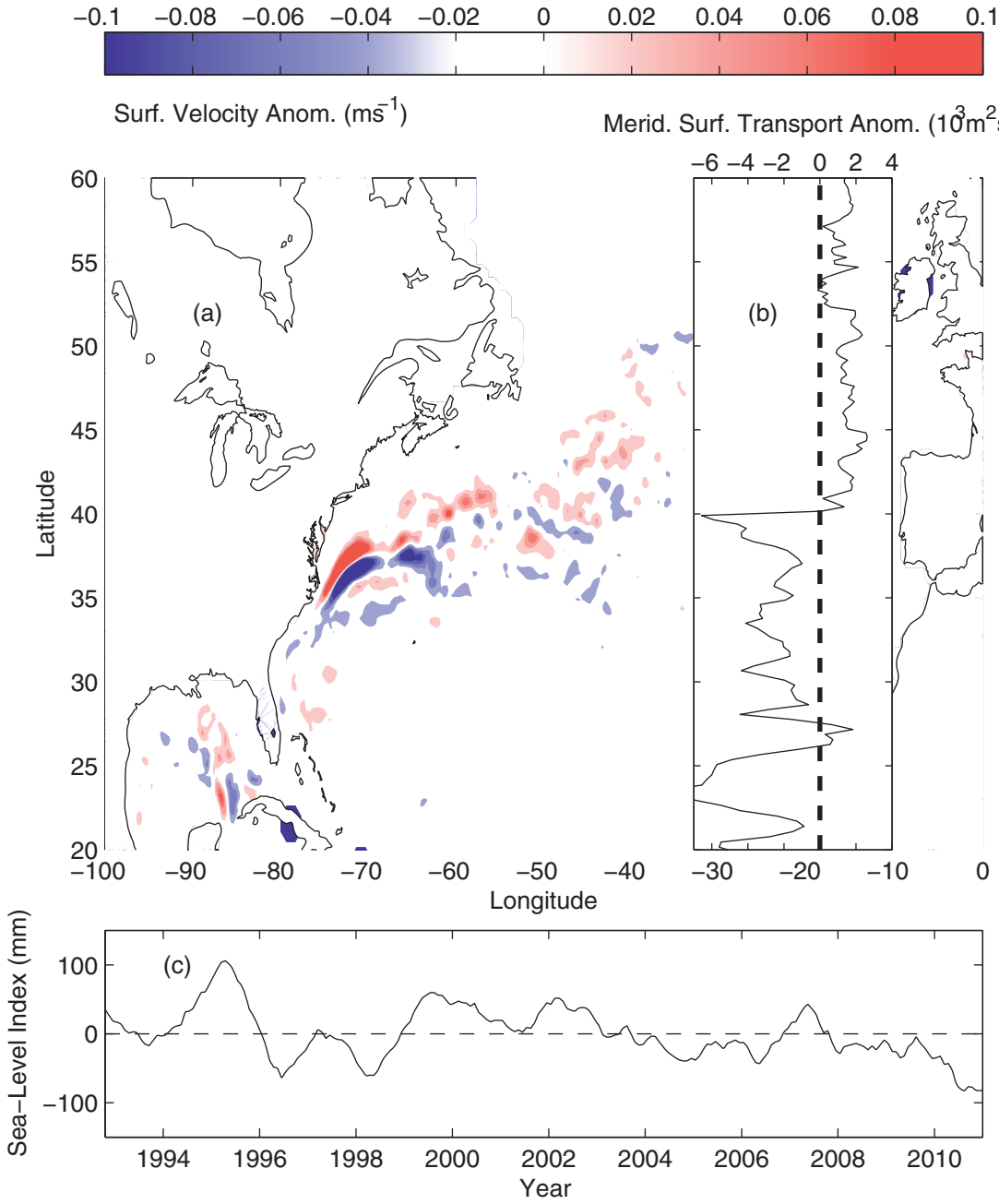

Extended Data Figure 4 | Surface velocity anomaly when the sea-level index is positive. **a**, Magnitude (m s^{-1}) and **b**, zonally integrated meridional velocity anomalies (10^3 m^2 s^{-1}) for the time period 1993 to 2011, corresponding to when (**c**) the sea-level index is positive. A positive sea-level index is associated with a more northerly circulation in the intergyre region and increased surface flow into the subpolar gyre. Velocities are geostrophic surface velocities derived from satellite altimetry.

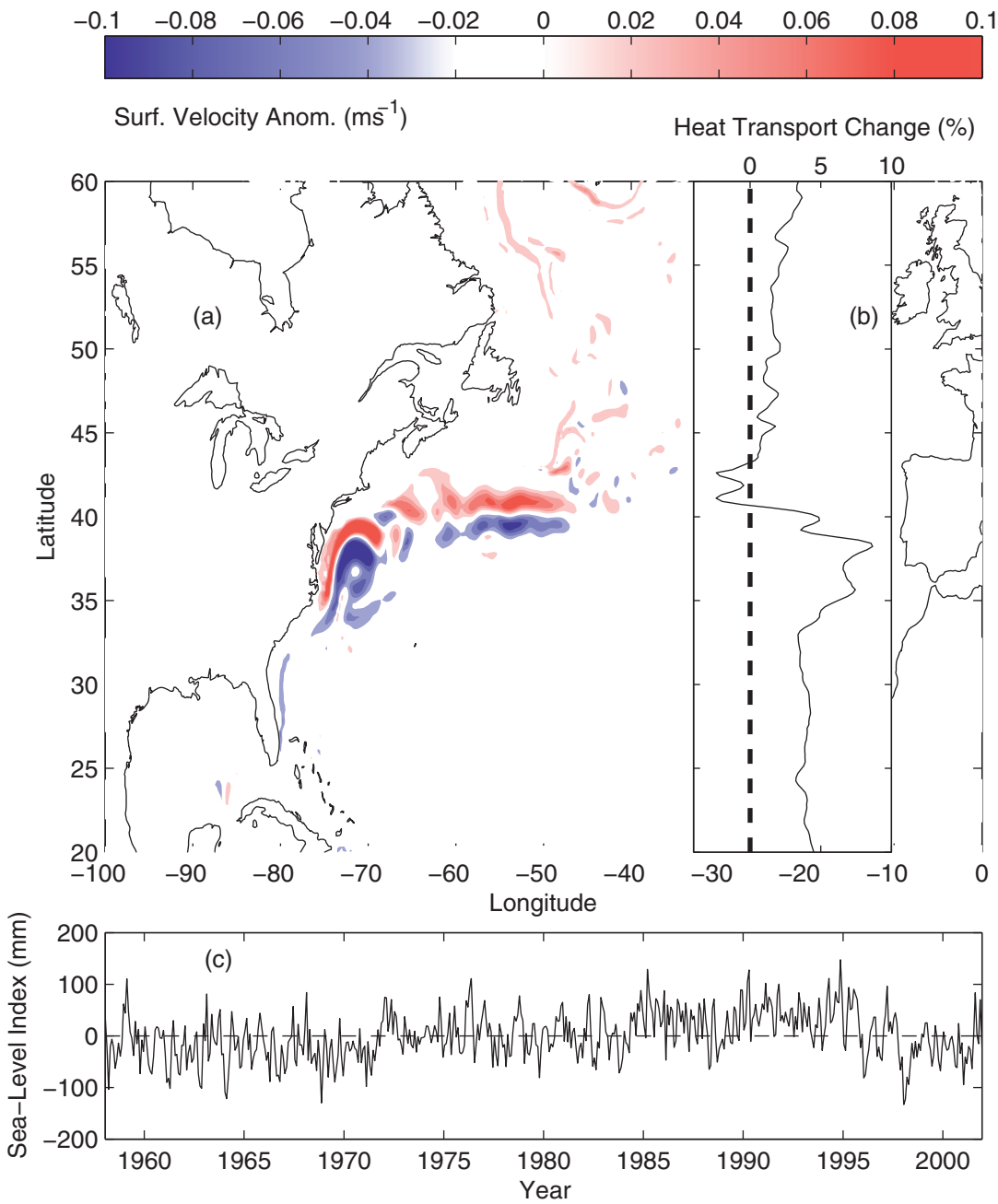

Extended Data Figure 5 | Model-derived surface velocity anomaly magnitude when the model-based sea-level index is positive. Similar to observed velocities, positive indices are associated with more northerly circulation in the intergyre region. **a**, Surface velocity magnitude (m s^{-1}) and **b**, percentage of meridional heat transport change (%) for the time period 1958 to 2001, corresponding to when (**c**) the model-derived sea-level index is positive. Similar to the satellite observations, a positive sea-level index is associated with a more northerly circulation in the intergyre region. Meridional heat transport change in both subtropical and subpolar gyres is positive when the sea-level index is positive.

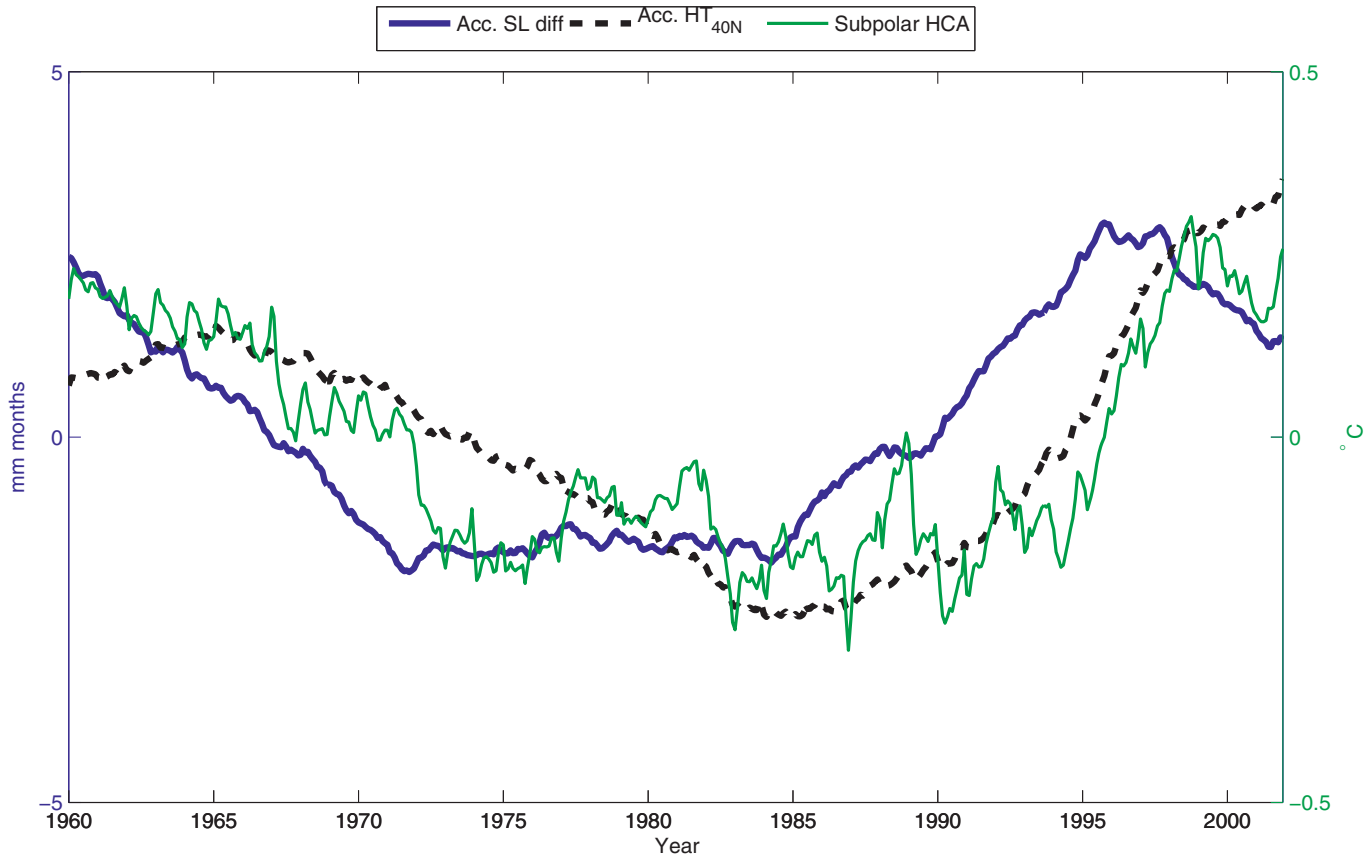

Extended Data Figure 6 | Model-derived sea-level index, heat transport and subpolar heat content. The accumulated sea-level index (Acc. SL diff, blue, in mm months) leads the accumulated heat transport into the subpolar gyre across 40° N (Acc. HT_{40N}, black, normalized units). The heat transport into the subpolar gyre dominates the top 500 m temperature anomaly (Subpolar HCA, green, °C) in the subpolar gyre.

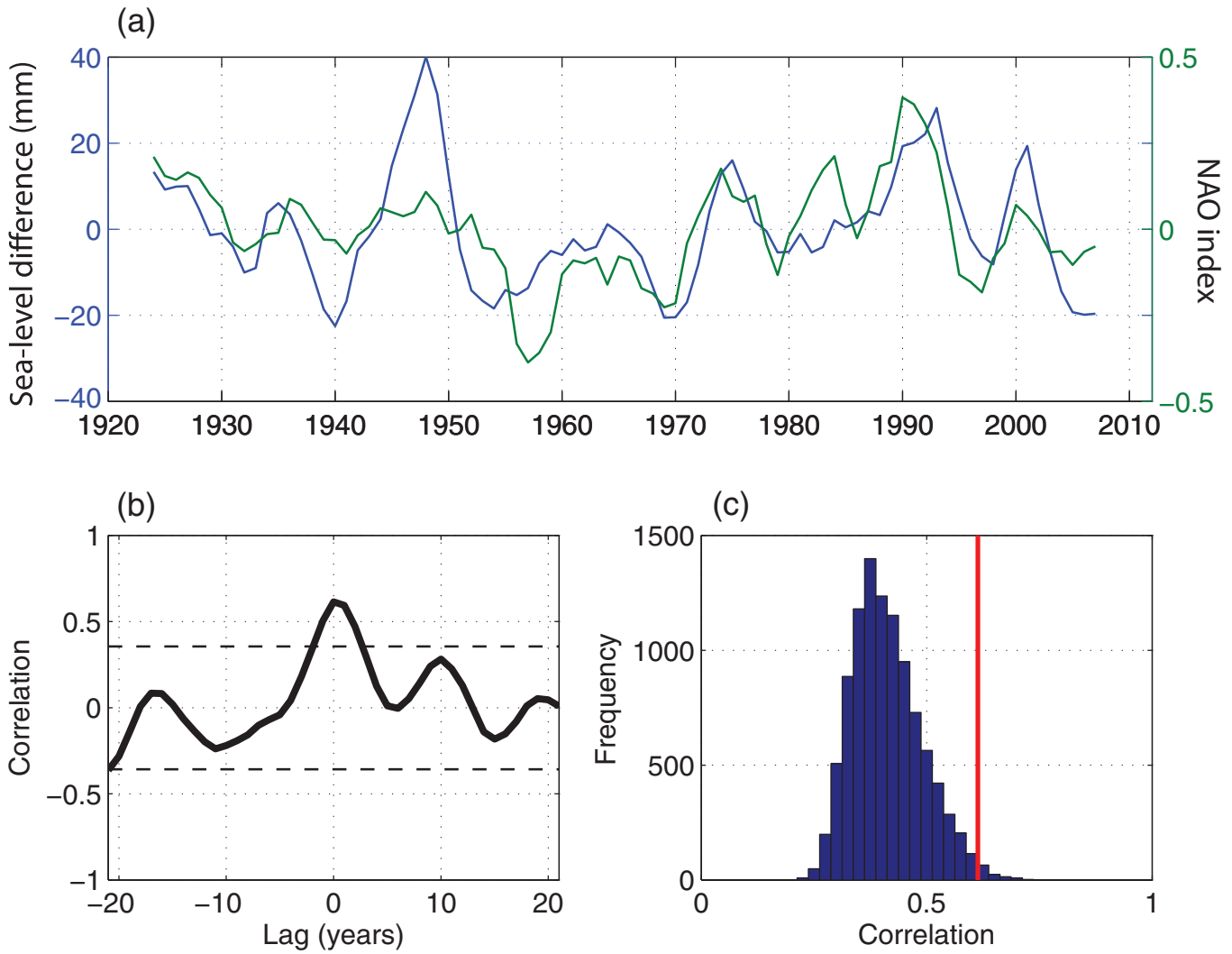

Extended Data Figure 7 | Relationship between sea-level index and the NAO. **a**, 7-year sea-level difference (blue, cm) and 7-year NAO (green, normalized units). **b**, Lagged correlations between the two quantities. **c**, Scrambled correlation tests. The histogram indicates the typical correlations that would be expected from randomly generated timeseries with similar spectral properties to the original timeseries. The red line indicates the maximum correlation between the two timeseries.

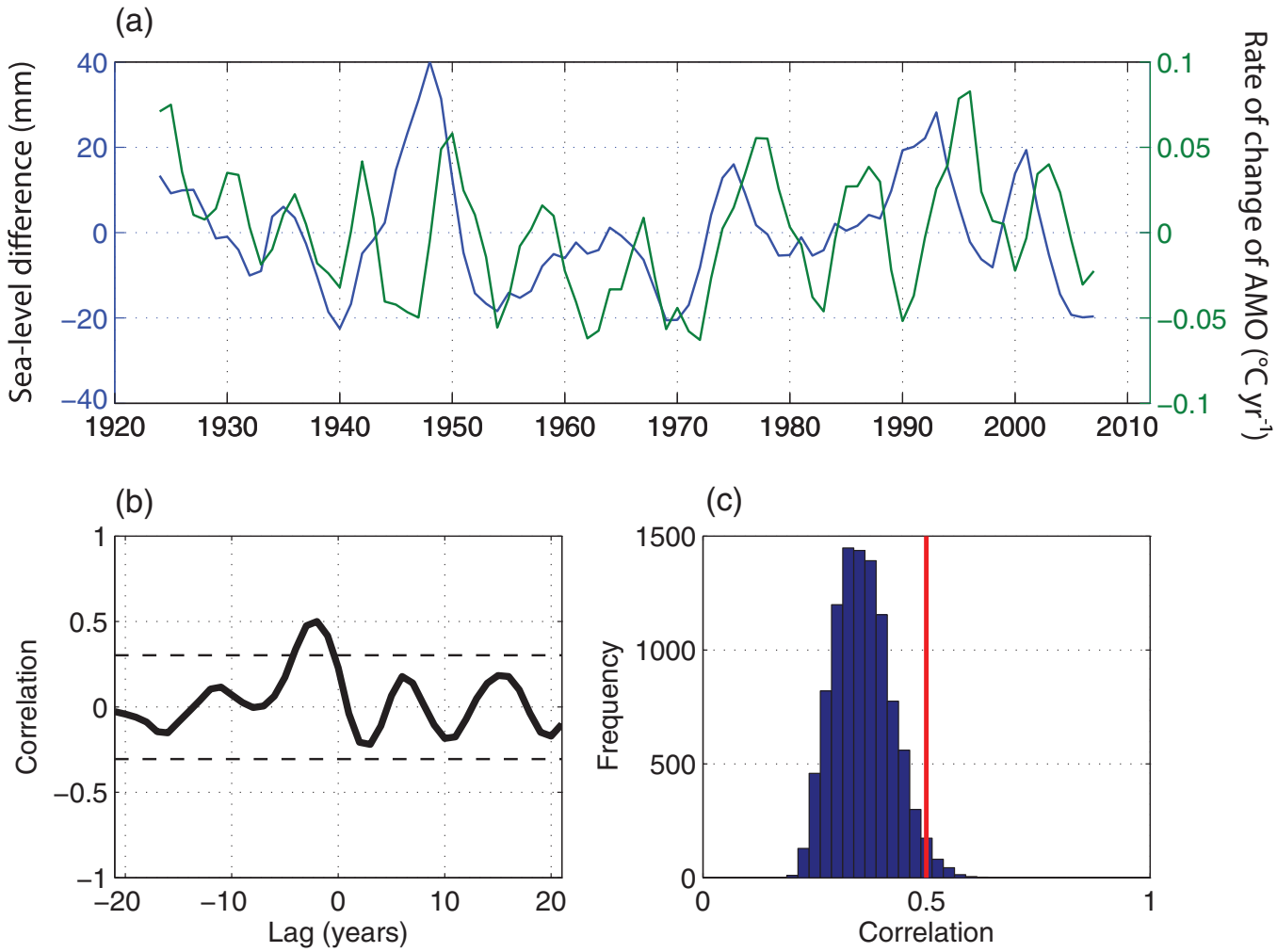

Extended Data Figure 8 | Relationship between sea-level index and the rate of change of the AMO. **a**, 7-year sea-level difference (blue) and rate of change of the AMO (green). **b**, Lagged correlations between the two quantities. **c**, Scrambled correlation tests. The histogram indicates the typical correlations that would be expected from randomly generated timeseries with similar spectral properties to the original timeseries. The red line indicates the maximum correlation between the two timeseries.

Extended Data Table 1 | Sea level, NAO and rates of change of the AMO statistics

Var X	Var Y	Filt (yrs)	Time interval	DoF	Corr	Sig. % (t-stat)	Sig. % (Scrm)	RMS of rand corr	Lag at max corr (yrs)	Estimated range of lag (yrs)
B-A	Di HC	7	1950-2012	9	0.58	95	98	0.22	-2	-3 to 0
B-A	NAO	7	1950-2012	9	0.71	98	98	0.29	1	-1 to 2
NAO	Di HC	7	1950-2012	9	0.41	86	84	0.18	-2	-4 to -1
B-A	NAO	7	1920-2012	13	0.61	98	99	0.21	0	-1 to 2
B	NAO	7	1920-2012	13	-0.50	95	86	0.23	-11	-13 to 7
A	NAO	7	1920-2012	13	-0.43	91	70	0.22	1	-3 to 4
B-A	Di AMO	7	1920-2012	13	0.51	96	98	0.18	-2	-4 to -1
NAO	Di AMO	7	1920-2012	13	0.58	98	98	0.21	-4	-5 to -2

Correlation, lags and significance between the southern (B) and northern (A) sea-level indices. First variable (Var X) and second variable (Var Y) are indicated in the first two columns. In the second column, Di refers to the rate of change, and HC refers to subpolar heat content from 40° to 60° N. All timeseries are filtered with a 7-year low-pass filter (Filt). Degrees of Freedom (DoF), correlation (Corr) and significance (Sig.) are shown. Significance is determined by a *t*-statistic (*t*-stat) or a scrambled test (Scrm). The RMS of a random correlation (column 9) together with the lag at maximum correlation (column 10) allows determination of a range for the lag estimate (column 11).

Extended Data Table 2 | Sub-sampled statistics

From	To	Correlation	Lag (yrs)	Lag range (yrs)
1920	2012	0.5	-2	-4 to -1
1920	1980	0.36	-1	-3 to 0
1936	1995	0.46	-3	-4 to -1
1952	2012	0.54	-2	-4 to 0

Correlation, lags and lag range of sea-level index and the rate of change of the AMO over various time periods to investigate the consistency of the lags. Time periods under consideration are indicated in the first two columns.